

1   **Where is the Io plasma torus? A comparison of observations by**  
2   **Juno radio occultations to predictions from Jovian magnetic**  
3   **field models**

4   **Phillip H. Phipps<sup>1</sup>, Paul Withers<sup>1,2</sup>, Marissa F. Vogt<sup>1</sup>, Dustin R. Buccino<sup>3</sup>, Yu-Ming Yang<sup>3</sup>,**  
5   **Marzia Parisi<sup>3</sup>, Drake Ranquist<sup>4</sup>, Peter Kollmann<sup>5</sup>, Scott Bolton<sup>6</sup>**

6   <sup>1</sup>Center for Space Physics, Boston University, Boston, MA, USA.

7   <sup>2</sup>Department of Astronomy, Boston University, Boston, MA, USA.

8   <sup>3</sup>Jet Propulsion Laboratory, California Institute of Technology, Pasadena, CA, USA.

9   <sup>4</sup>Laboratory for Atmospheric and Space Science, University of Colorado Boulder,  
10   Boulder, CO, USA.

11   <sup>5</sup>The Johns Hopkins University Applied Physics Lab, Laurel, MD, USA.

12   <sup>6</sup>Southwest Research Institute, San Antonio, TX, USA.

13   **Key Points:**

- 14   • The location of the Io plasma torus depends on longitude and radial distance.
- 15   • Observed torus locations are predicted better by the JRM09 model than by the  
16    VIP4 model.
- 17   • The predicted location of the “torus beyond  $5.5 R_J$ ” improves if a current sheet  
18    model is included.

19      **Abstract**

20      The Io plasma torus is thought to lie in Jupiter's centrifugal equator, a location that de-  
 21      pends on Jupiter's rotation and magnetic field. Yet previous observations and predictions  
 22      of the location of the Io plasma torus are inconsistent. Here we test the hypothesis that  
 23      the Io plasma torus lies in the centrifugal equator by comparison of observations by Juno  
 24      radio occultations to predictions derived from Juno-era magnetic field models. These ob-  
 25      servations determine the locations of two torus components: the cold torus, which is cen-  
 26      tered near 5.3 Jovian radii ( $R_J$ ), and the "torus beyond  $5.5 R_J$ ", which is dominated by  
 27      the warm torus and is centered near  $5.9 R_J$ . The observations deviate by 1–2 degrees  
 28      from the planar centrifugal equator expected for a Voyager epoch dipolar magnetic field.  
 29      In each observation, the locations of distinct torus regions differ by as much as 1 degree  
 30      indicating significant radial structure. The root-mean-square error between observation  
 31      and prediction is smaller for predictions from the JRM09 magnetic field model than for  
 32      predictions from the VIP4 magnetic field model. Agreement between observations and  
 33      predictions improves for the "torus beyond  $5.5 R_J$ " if the magnetic field contributions of a  
 34      nominal magnetospheric current sheet model are included, but worsens for the cold torus.  
 35      The current sheet affects the location of the "torus beyond  $5.5 R_J$ ", but not the cold torus  
 36      at  $5.3 R_J$ . Improved knowledge of the torus location will help to understand how the torus  
 37      affects the broader magnetosphere.

38      **1 Introduction**

39      The innermost Galilean satellite, Io, is the source of most of the material in Jupiter's  
 40      magnetosphere. This material, made mostly of sulfur and oxygen atoms, gets ionized and  
 41      trapped by Jupiter's magnetic field [Thomas *et al.*, 2004]. The ionized material is trans-  
 42      ported radially through the magnetosphere. The plasma is then lost via charge exchange  
 43      with neutrals or transported to the outer magnetosphere. The highest density of the plasma  
 44      lies between 5 and 10 Jovian radii (1 Jovian radius = 71,492 km,  $R_J$ ) in what is called the  
 45      Io plasma torus (IPT).

46      These charged particles are trapped on magnetic field lines. Yet this plasma does  
 47      not drift freely along the full pole-to-pole extent of a field line. Instead, centrifugal forces  
 48      caused by Jupiter's rapid rotation confine plasma near the point of minimum centrifugal  
 49      potential, which is the point on the field line that is farthest from Jupiter's rotational axis  
 50      [Hill *et al.*, 1974; Vasyliunas, 1983; Khurana *et al.*, 2004; Thomas *et al.*, 2004]. The col-  
 51      lection of the maximally separated points on Jupiter's field lines is called the "centrifugal  
 52      equator".

53      If the magnetic field is dipolar, then the centrifugal equator is a plane. However, if  
 54      higher-order moments contribute to the magnetic field, then the shape of the surface of the  
 55      centrifugal equator is distorted from a plane [e.g., Schneider and Trauger, 1995]. Indeed,  
 56      observations have suggested that the Io plasma torus appears "warped like a potato chip"  
 57      [Herbert *et al.*, 2008], consistent with the centrifugal equator having a non-planar shape.  
 58      Furthermore, ground-based imaging observations of the location of the Io plasma torus by  
 59      Schneider and Trauger [1995] were reproduced better by centrifugal equator predictions  
 60      based on high-order models of that time, the O4 and O6 models [Acuna and Ness, 1976;  
 61      Connerney *et al.*, 1981; Connerney, 1993], than by a simple offset tilted dipole model.  
 62      Using Voyager data, Bagenal [1994] showed that the predicted location of the torus inward  
 63      of  $5.5 R_J$  was very sensitive to the magnetic field model used and that the O4 and O6  
 64      models were not adequate.

65      Based on these results from the Voyager epoch, observations and predictions of the  
 66      location of the Io plasma torus are inconsistent. This inconsistency is significant. In or-  
 67      der to understand the behavior of Jupiter's magnetosphere, the largest object in the Solar  
 68      System, it is necessary to understand the behavior of the Io plasma torus, which is the  
 69      source of most plasma in Jupiter's magnetosphere. In order to understand the behavior

70 of the Io plasma torus, it is necessary to understand where in the magnetosphere the Io  
71 plasma torus is located.

72 Three main hypotheses exist that could resolve this problem: the observations are  
73 insufficient, the predictions are insufficient, or the basic premise that the Io plasma torus  
74 lies in the centrifugal equator is insufficient. Since the Voyager epoch, new information  
75 has been acquired by the Juno spacecraft that can be used to address this problem. Ra-  
76 dio occultations by Juno have sampled the electron density distribution within the torus,  
77 yielding precise measurements of the location of the Io plasma torus. Magnetic field mea-  
78 surements by Juno have sampled closer to Jupiter and over a wider range of latitudes than  
79 before, yielding an improved model of the internal magnetic field of Jupiter. This leads to  
80 an improved prediction for the location of the centrifugal equator.

81 The aim of this article is to test the hypothesis that the Io plasma torus lies in the  
82 centrifugal equator. This aim is achieved by the comparison of observations by Juno radio  
83 occultations to predictions derived from Juno-era magnetic field models. Section 2 de-  
84 scribes the available Juno radio occultation observations of the location of the Io plasma  
85 torus. Section 3 describes selected internal and external magnetic field models and their  
86 predictions for the location of the Io plasma torus. The internal field is generated within  
87 Jupiter. The external field is generated in the magnetosphere, primarily in the current  
88 sheet. Section 4 compares observed and predicted locations of the Io plasma torus. Sec-  
89 tion 5 assesses the impact of plausible variations in the poorly constrained parameters of  
90 the external field on the predicted location of the Io plasma torus. Section 6 interprets the  
91 results of Sections 4-5. Section 7 states the conclusions of this article.

## 92 **2 Observations by Juno radio occultations**

93 The Juno spacecraft entered orbit around Jupiter on 4 July 2016. Its orbital period  
94 has remained constant at approximately 53 days. During each perijove, the Juno–Earth  
95 line of sight sweeps through one sector of the IPT. Operations on some, but not all, per-  
96 ijoves have a gravity science focus. During the first two years of the Juno Mission grav-  
97 ity science observations were performed on Perijoves 1, 3, 6, 8, 10, 11, 13, 14, and 15.  
98 During those perijoves, Juno points its high-gain antenna towards Earth and maintains  
99 a two-way coherent radio link with a ground station of the NASA Deep Space Network  
100 (DSN) at X-band and Ka-band frequencies. These X-band and Ka-band radio signals pass  
101 through the Io plasma torus, which affects their observed differential Doppler shift. A  
102 time series of the total electron content along the Juno–Earth line of sight can be deter-  
103 mined from such observations. As the path of the Juno–Earth line of sight through the  
104 IPT changes with time during each perijove, this provides information on the spatial dis-  
105 tribution of plasma in the Io plasma torus. During the other Juno perijoves, radio signals  
106 are transmitted from Juno’s medium gain antenna and are thus much noisier and are un-  
107 suitable for the purpose of determining densities in the Io plasma torus. Thus, data from  
108 Perijoves 2, 4, 5, 7, 9, and 12 are not suitable for Io plasma torus studies.

109 As explained in detail in *Phipps et al. [2018]* and *Phipps et al. [2019]*, the observed  
110 differential Doppler shift is integrated with respect to time to yield an initial time series  
111 of the total electron content (TEC) along the Juno–Earth line of sight. This contains sev-  
112 eral contributions from sources other than the Io plasma torus, such as Earth’s ionosphere  
113 and the solar wind, which should be removed from the initial time series of TEC. First,  
114 contributions from Earth’s ionosphere are subtracted from the initial time series of TEC  
115 to obtain the intermediate time series of TEC. This uses the line of sight total electron  
116 content of Earth’s ionosphere, which is provided by a routine DSN data product measured  
117 using radio links to GPS satellites visible above the DSN stations. Second, contributions  
118 from changes in the solar wind are subtracted from the intermediate time series of TEC  
119 to obtain the final time series of TEC. The intermediate time series of TEC still contains  
120 a contribution from changes in the TEC in the solar wind along the Juno–Earth line of

sight. This is not directly measurable. Instead, a high-order polynomial function of time is fitted to the intermediate TEC values at times outside the interval of the Io plasma torus occultation. This baseline function is subtracted from the intermediate time series of TEC to obtain the final time series of TEC. Note that the steady state value of the solar wind TEC does not affect the observations.

The final time series of TEC is expressed as a one-dimensional function of position, where the relevant position coordinate for each Earth received time is a distance above the nominal plane of the centrifugal equator. Specifically, the distance above the nominal plane of the centrifugal equator of the point on that ray path whose projected distance from Jupiter in the nominal plane of the centrifugal equator is  $5.89 R_J$ , the orbital distance of Io.

The Io plasma torus consists of three distinct regions: the cold torus ( $4.9\text{--}5.5 R_J$ ), ribbon ( $5.5\text{--}5.7 R_J$ ), and warm torus ( $5.7\text{--}8 R_J$ ) [Bagenal and Sullivan, 1981; Thomas *et al.*, 2004; Phipps, 2019]. Values of the peak total electron content, the offset of the location of peak total electron content from the centrifugal equator, and the scale height are found for two components of the torus by fitting a pair of Gaussian functions of position to the final TEC values. The location of peak total electron content can be expressed as an angular offset from an idealized planar centrifugal equator expected for a dipolar magnetic field. The two fitted components of the torus are the cold torus and the torus beyond  $5.5 R_J$ , where the latter includes contributions from the warm torus and the ribbon. Representative radial distances of the two fitted regions are  $5.3 R_J$  and  $5.9 R_J$ . The “torus beyond  $5.5 R_J$ ” region contains the ribbon and warm torus, but is likely dominated by total electron content contributions from the warm torus. The Juno observations are not able to discriminate between the warm torus and ribbon, which have similar scale heights.

Results of Juno radio occultation observations of the Io plasma torus have been reported by Phipps *et al.* [2018] and Phipps *et al.* [2019] for four Juno perijoves (PJ). These are PJ1 ( $\lambda_{III} = 184$  degrees, 27 August 2016), PJ3 ( $\lambda_{III} = 60$  degrees, 11 December 2016), PJ6 ( $\lambda_{III} = 213$  degrees, 19 May 2017), and PJ8 ( $\lambda_{III} = 10$  degrees, 1 September 2017). The locations of two components of the Io plasma torus were determined by Phipps and colleagues for these four observations. The fitted locations and their uncertainties from Phipps *et al.* [2018] and Phipps *et al.* [2019] are shown in Table 2. Io plasma torus properties from Perijoves 10, 11, 13, 14, and 15 have not yet been determined.

The dependence of the fitted locations on longitude is shown in Figure 1. The observed locations generally deviate by 1–2 degrees from the idealized planar centrifugal equator expected for a dipolar magnetic field from the Voyager epoch. This can be seen by the offset from zero of the observations in Figure 1. This confirms that the centrifugal equator is not planar. On any given perijove, the locations of the cold torus and the torus beyond  $5.5 R_J$  differ by as much as 1 degree, indicating that significant radial structure is present in the centrifugal equator between  $5.3$  and  $5.9 R_J$ .

### 3 Predictions based on magnetic field models

Predictions for the location of the centrifugal equator rely upon magnetic field models. Jupiter possesses the strongest magnetic field of any planet in the solar system [Bagenal, 2013; Kivelson and Bagenal, 2014]. Although the planet’s internally-generated field is predominantly dipolar, significant spectral power is present in the higher-order moments [Connerney *et al.*, 2018]. Several models of Jupiter’s internal magnetic field have been generated by analysis of magnetic field measurements and other constraints [Acuna and Ness, 1976; Connerney, 1993; Connerney *et al.*, 1998; Grodent *et al.*, 2008; Hess *et al.*, 2011; Connerney *et al.*, 2018].

There are also external magnetic fields created by currents in the magnetosphere (e.g. ring current, magnetopause current, current sheet) [Khurana *et al.*, 2004]. For the re-

171 gion of the magnetosphere from  $5 R_J$  to  $40 R_J$ , the most significant external field comes  
 172 from the current sheet. Jupiter's magnetosphere is full of plasma which is confined in a  
 173 sheet in the outer magnetosphere. Currents flow through this confined plasma leading to  
 174 the creation of magnetic fields [see review by *Khurana et al.*, 2004]. These currents are  
 175 closed in the ionosphere of Jupiter and lead to magnetosphere-ionosphere coupling and  
 176 Jupiter's powerful aurora. This current sheet originates near the orbit of Io, the source  
 177 of the bulk of the plasma in the magnetosphere. Despite the strength of Jupiter's internal  
 178 magnetic field, the external magnetic field is not negligible in the regions outside of  $5.5 R_J$ .  
 179 Previous studies have shown that these external magnetic fields have appreciable influence  
 180 on the magnetic field environment around the Io plasma torus [*Connerney et al.*,  
 181 1981; *Khurana*, 1992, 1997]. Current sheet models have been developed to fit data from  
 182 Voyager and Galileo [*Connerney et al.*, 1981; *Khurana*, 1992, 1997].

### 183 3.1 Internal field models

184 We consider two internal magnetic field models: the widely-used VIP4 internal field  
 185 model [*Connerney et al.*, 1998], which is based upon Pioneer 11 and Voyager 1 magne-  
 186 tometer data, plus optical observations of the location of the Io auroral footprint; and the  
 187 recent JRM09 internal field model [*Connerney et al.*, 2018], which is based upon the first  
 188 nine orbits of magnetometer data acquired by the Juno magnetic field investigation.

189 Both the VIP4 and JRM09 models adopt a spherical harmonic representation of the  
 190 field. The planetary magnetic field can be defined as the gradient of a scalar potential,  
 191  $\vec{B} = \vec{\nabla}V$ . The scalar potential is defined by a spherical harmonic expansion of the follow-  
 192 ing form [e.g *Chapman and Bartels*, 1940; *Connerney et al.*, 1998, 2018]:

$$193 V = a \sum_{n=1}^{n_{max}} \left(\frac{a}{r}\right)^{n+1} \sum_{m=0}^n \{P_n^m(\cos \theta) [g_n^m \cos m\phi + h_n^m \sin m\phi]\} \quad (1)$$

194 where  $a$  is the equatorial radius of Jupiter,  $r$  is the radial distance to the planet's center,  
 195 angle  $\theta$  is the colatitude, and angle  $\phi$  is the longitude. The  $P_n^m(\cos \theta)$  are the Schmidt-  
 196 normalized associated Legendre functions of degree  $n$  and order  $m$ . The coefficients  $g_n^m$   
 and  $h_n^m$  are the fitted internal field parameters called Schmidt coefficients.

197 Magnetometer data can be fitted to the scalar potential representation of the mag-  
 198 netic field to determine the coefficients for the field. The field models for Jupiter are found  
 199 as a partial solution to a linearized system [*Connerney*, 1981]. The dipole parameters,  
 200 dipole moment ( $M$ ), dipole tilt ( $\theta_M$ ), and orientation ( $\lambda_M$ ), are determined using the  $g_1^0$ ,  
 201  $g_1^1$ , and  $h_1^1$  coefficients as follows [*Khurana et al.*, 2004]:

$$M = \sqrt{(g_1^0)^2 + (g_1^1)^2 + (h_1^1)^2} \quad (2)$$

$$\theta_M = \tan^{-1} \left( \sqrt{(g_1^1)^2 + (h_1^1)^2} / g_1^0 \right) \quad (3)$$

$$\lambda_M = \tan^{-1} \left( h_1^1 / g_1^1 \right). \quad (4)$$

202 The VIP4 internal field model stands for Voyager, Io, and Pioneer 4th order model [*Con-*  
 203 *nerney et al.*, 1998]. The dipole parameters determined for this model are  $M = 4.264$   
 204 Gauss,  $\theta_M = 9.5$  degrees, and in System III (1965) West coordinates  $\lambda_M = 200.8$  degrees.  
 205 In this article we use System III (1965) West.

206 The JRM09 internal field model stands for "Juno Reference Model through Perijove  
 207 9" [*Connerney et al.*, 2018]. This model uses observations from the Juno spacecraft made  
 208 within  $7 R_J$  of Jupiter during the first 9 orbits. This model also calculates the spherical  
 209 harmonic expansion through degree 20 but values are only well defined through degree

210    10. The dipole parameters determined for this model are  $M = 4.170$  Gauss,  $\theta_M = 10.31$   
 211    degrees, and in System III (1965) West coordinates  $\lambda_M = 196.61$  degrees.

212    In this article, we use the VIP4 dipole parameters to define the idealized planar cen-  
 213    trifugal equator expected for a dipolar magnetic field. This is used as the reference from  
 214    which angular offsets are measured. This convention is adopted for consistency with the  
 215    reference Io torus models of *Phipps and Withers* [2017], *Phipps et al.* [2018], and *Phipps*  
 216    *et al.* [2019]. The JRM09 dipole parameters are stated for reference only.

217    Even though VIP4 ends at 4<sup>th</sup> order and JRM09 truncates at 10<sup>th</sup> order, further  
 218    truncated versions of the VIP4 and JRM09 internal field models can also be generated  
 219    in which coefficients above some threshold degree are ignored. For example, a dipole ap-  
 220    proximation to such a model arises from neglecting all coefficients above degree 1. Sim-  
 221    ilarly, a fourth-order approximation arises from neglecting all coefficients above degree 4.  
 222    The parameters for the dipole approximation to each model can be found in Table 1.

### 223    3.2 External field models

224    Previous studies have adopted two primary methods for modeling the external field  
 225    produced by the magnetospheric current sheet. The first method to model the current  
 226    sheet was applied by *Connerney et al.* [1981]. Similar to the internal field, they solved for  
 227    an analytical solution for a potential to match Voyager 1 and 2 and Pioneer 10 observa-  
 228    tions of the current sheet. However, unlike the internal field, they solved for a vector po-  
 229    tential  $\vec{A}$  that satisfies the relation  $\vec{B} = \nabla \times \vec{A}$ . From this relation, *Connerney et al.* [1981]  
 230    derived simple analytical functions, assuming the current sheet is azimuthally symmetric,  
 231    which approximate the solution and allow fast computation of the field. This model does  
 232    a reasonable job between  $6 R_J$  and  $30 R_J$ . However, after  $30 R_J$  there is hinging and lag  
 233    behind co-rotation of the current sheet, which breaks the symmetric approximation [*Khur-  
 234    rana et al.*, 2004]. The abrupt inner edge of this current sheet model at  $5 R_J$  also leads  
 235    to fringing effects inside  $5 R_J$  [Vasyliunas, 1983]. Despite these issues, the model does a  
 236    reasonable job matching measurements between 5 and  $8 R_J$ , where the Io plasma torus is  
 237    located. An updated version of this current sheet has been published by *Pensionerov et al.*  
 238    [2019]. The updated current sheet model of *Pensionerov et al.* [2019] starts from the same  
 239    functional form as *Connerney et al.* [1981], then adds two additional terms to capture the  
 240    deviations between observations and model beyond around  $30 R_J$ . It also updates the pa-  
 241    rameters that define the model.

242    The second method uses Euler potentials to derive the magnetic field. This method  
 243    uses two scalar functions to represent the magnetic field. *Goertz* [1976] derived a scalar  
 244    potential  $f$  that is dependent on radial distance and height above the plane and a scalar  
 245    potential  $g$  that is dependent on radial distance and azimuthal angle. This method was  
 246    improved upon by *Khurana* [1997] to allow the internal and current sheet models to be  
 247    linked. This model was created using dawn side data and thus does a reasonable job in  
 248    that sector. The *Khurana* [1997] model included the hinging and lag of the magnetic field  
 249    beyond  $30 R_J$  to better map the field in the outer magnetosphere.

250    Here we adopt the current sheet model of *Connerney et al.* [1981] (called CAN). It  
 251    provides reasonable agreement with magnetic field measurements at the radial distances  
 252    of the Io plasma torus. The current sheet model of *Pensionerov et al.* [2019] has the same  
 253    functional form as CAN at the radial distances of the Io plasma torus. *Pensionerov et al.*  
 254    [2019] updated the model parameters given by *Connerney et al.* [1981], but the conclu-  
 255    sions of our analysis are not sensitive to the precise values of the model parameters that  
 256    are adopted (Section 5). The model of *Khurana* [1997] is optimized for the dawn sector,  
 257    whereas Juno radio occultation observations sample the noon sector. Furthermore, its so-  
 258    phisticated representations of hinging and associated behavior are primarily relevant for  
 259    the outer magnetosphere, not the radial distances of the Io plasma torus.

The parameters of the CAN current sheet model are listed at the bottom of Table 1. Figure 2 shows the relationship between the total magnetic field strength of the JRM09, JRM09 dipole, JRM09 greater than dipole (quadrupole and above), the CAN current sheet, and the JRM09 plus current sheet models in the magnetic equator at a System III West longitude of 196.6 degrees.

### 3.3 The Centrifugal Equator

If the magnetic field is perfectly dipolar, then the location of the centrifugal equator at a given longitude satisfies [Hill *et al.*, 1974; Vasylunas, 1983; Khurana *et al.*, 2004; Phipps, 2019]:

$$\tan \theta = \frac{-4/3 \tan \alpha \cos \phi}{1 \mp \sqrt{1 + 8/9 \tan^2 \alpha \cos^2 \phi}} = \frac{-4/3 \tan \alpha \cos (\lambda_{III} - \lambda_M)}{1 \mp \sqrt{1 + 8/9 \tan^2 \alpha \cos^2 (\lambda_{III} - \lambda_M)}} \quad (5)$$

where  $\theta$  is the angle from the rotational equator to the centrifugal equator,  $\alpha$  is the tilt of the magnetic dipole axis from the planet's rotational axis, and  $\phi$  is the right-handed magnetic longitude. Jovigraphic longitude,  $\lambda_{III}$ , is the left-handed System III longitude and  $\lambda_M$  is the jovigraphic longitude of the magnetic prime meridian. These are related by  $\lambda_{III} - \lambda_M = 360^\circ - \phi - \lambda_M$ . Note that Equation 5 predicts that the angular location of the centrifugal equator is independent of radial distance for a dipolar magnetic field. The theoretical expression shown in Equation 5 is a useful benchmark for assessing predictions of non-dipolar magnetic field models for the location of the centrifugal equator, which may vary with radial distance. As discussed in Section 3.1, in the dipolar approximation to the VIP4 internal field model,  $\alpha$  is 9.6 degrees,  $\lambda_M$  is 200.8 degrees, and the predicted location of the centrifugal equator is as shown in Figure 3. The greatest absolute value of  $\theta$  is 6.4 degrees or  $2\alpha/3$ , consistent with the approximation to Equation 5 that  $\tan \theta = -2/3 \tan \alpha \cos \phi$  in the limit of small  $\alpha$ . A schematic of the centrifugal equator relative to the rotational and magnetic equators in the dipolar approximation is shown in Figure 4.

We find the centrifugal equator of a given magnetic field model by tracing a set of model field lines using the model parameters and identifying the point on each field line that is farthest from Jupiter's rotational axis. The field line is traced starting at a latitude of 0 degrees and moving toward the planet along the magnetic field. The tracing is done for longitudes from 0 to 360 degrees incrementing by 10 degrees and radial distances from 5 to 10  $R_J$  incrementing by 0.1  $R_J$ . The implementation of this approach is verified by reproduction of the analytical result shown in Figure 3 for the dipolar approximation to the VIP4 internal field model. Note that all subsequent descriptions of the location of the centrifugal equator are referenced to the dipolar approximation to the VIP4 internal field model, not to the rotational equator. This convention is adopted in order to highlight small differences effectively and to maintain consistency with previous work. Figure 5 shows the offsets from the dipolar approximation to the VIP4 internal field model for the VIP4 full model, the JRM09 dipolar approximation, the JRM09 truncated at 4th order, and the full JRM09 model.

The offsets of the centrifugal equator predicted by the full VIP4 internal field model from the dipolar approximation to the VIP4 model are shown in panel A of Figure 5. Deviations of this predicted centrifugal equator from the predicted centrifugal equator of the dipolar approximation to the VIP4 internal field model have a magnitude on the order of 1 degree. The longitudinal structure of these deviations is characterized by two maxima and two minima, each separated by 90 degrees in longitude. This shows that this predicted centrifugal equator is not planar. This predicted shape is similar to the "potato chip" shape seen in Io plasma torus observations [Schneider and Trauger, 1995; Herbert *et al.*, 2008]. Neither the two maxima nor the two minima of the tilt angle offsets are identical; slight asymmetries between them are present. Furthermore, slight variations with radial distance

307 are also apparent. No such variations with radial distance are possible in a purely dipolar  
 308 field model.

309 The offsets of the centrifugal equator predicted by the dipolar approximation to the  
 310 JRM09 internal field model from the dipolar approximation to the VIP4 model are shown  
 311 in panel B of Figure 5. In this instance,  $\alpha$  is 10.31 degrees and  $\lambda_M$  is 196.61 degrees,  
 312 slightly different from the corresponding values above for the VIP4 internal field model.  
 313 Results are shown for different radial distances even though no dependence on radial dis-  
 314 tance exists in this dipolar case. This is done for consistency with the other panels of Fig-  
 315 ure 5 and later figures. The basic shape of the difference between the centrifugal equators  
 316 of the dipolar approximations to the JRM09 and VIP4 internal field models is consistent  
 317 with the difference between two tilted planes. The maximum value of the difference, 0.72  
 318 degrees, is consistent with the difference between tilts of 6.4 degrees and 6.9 degree (two-  
 319 thirds of the respective values of  $\alpha$ ). Note that this is not equivalent to the difference in  
 320 magnetic dipole axis tilt due to a shift in longitude between the models.

321 The offsets of the centrifugal equator predicted by a JRM09 internal field model that  
 322 is truncated at degree 4 from the dipolar approximation to the VIP4 model are shown in  
 323 panel C of Figure 5. The offsets of the centrifugal equator predicted by the full JRM09  
 324 internal field model from the dipolar approximation to the VIP4 model are shown in panel  
 325 D of Figure 5. Differences between these two are negligible, which shows that terms  
 326 above degree 4 can be neglected in this analysis. Hence we focus on interpretation of the  
 327 JRM09 internal field model truncated at degree 4 in the remainder of this article, setting  
 328 aside the full JRM09 internal field model which is computationally more difficult to run  
 329 due to the higher order terms. This predicted centrifugal equator is qualitatively similar  
 330 to that of the full VIP4 internal field model (panel A). However, differences between the  
 331 centrifugal equators predicted by these two degree 4 models are present. For example,  
 332 the asymmetry between the two tilt angle offset minima is greater in the JRM09 internal  
 333 field model than in the VIP4 internal field model. These differences can be attributed to  
 334 the differences in the fitted dipolar tilt and tilt longitude values for the two models. These  
 335 fitted dipole values differ between the VIP4 and JRM09 models due to the different data  
 336 used in the two models. Figure 6 shows the dependence of offset on longitude for each of  
 337 the four models in panels A–D of Figure 5. Values are shown for a distance of  $6 R_J$ .

#### 338 4 Comparison of observations and predictions

339 The top panel of Figure 7 shows how the four observed locations of the cold torus  
 340 and the four observed locations of the torus beyond  $5.5 R_J$  compare to the locations of  
 341 the centrifugal equator predicted by the full VIP4 internal field model. The error bars are  
 342 the one sigma uncertainties on the measurements from *Phipps et al. [2018]* and *Phipps*  
 343 *et al. [2019]*. They are also listed in Table 2. The observed locations generally deviate  
 344 from the plane of the dipolar approximation to the VIP4 internal field model and (not  
 345 shown) the plane of the dipolar approximation to the JRM09 internal field model by 1–  
 346 2 degrees, confirming that the centrifugal equator is not planar. On any given perijove, the  
 347 locations of the cold torus and the torus beyond  $5.5 R_J$  differ by as much as 1 degree, in-  
 348 dicating that significant radial structure is present in the centrifugal equator between  $5.3$   
 349 and  $5.9 R_J$ . Yet neither the cold torus observations nor the torus beyond  $5.5 R_J$  observa-  
 350 tions lie close to the VIP4 prediction for the centrifugal equator.

351 The middle panel of Figure 7 compares the observed locations to the centrifugal  
 352 equator predicted for the truncated JRM09 internal field model. The observed cold torus  
 353 locations are consistent with the centrifugal equator predicted for the truncated JRM09  
 354 internal field model. Yet the observed locations of the torus beyond  $5.5 R_J$  are not consis-  
 355 tent with these predictions.

356 Two interpretations are possible: either the torus beyond  $5.5 R_J$  does not lie in the  
 357 centrifugal equator or the JRM09 internal field model does not accurately predict the lo-  
 358 cation of the centrifugal equator at distances of  $5.9 R_J$ , despite being successful at the  
 359 nearby distance of  $5.3 R_J$ . In fact, neither the VIP4 internal field model nor the JRM09  
 360 internal field model predicts a  $\sim 1$  degree change in location of the centrifugal equator as  
 361 observed on PJ8 (10 degrees longitude) and on PJ1 (184 degrees longitude) at any longi-  
 362 tude. This suggests that the problem is more subtle than some coefficient values being in-  
 363 correct. It is inherently difficult for models of this type to yield variations over such short  
 364 spatial scales far from the currents that generate the fields.

365 That realization points to a likely resolution of this problem. The VIP4 and JRM09  
 366 internal field models represent the internally-generated magnetic field of Jupiter. They do  
 367 not include representations of contributions from the magnetospheric current sheet [*Con-*  
 368 *nerney et al.*, 1981]. Therefore we add a model of currents in Jupiter's magnetosphere to  
 369 the truncated JRM09 internal field model. Jupiter's magnetospheric current sheet is mostly  
 370 confined to equatorial latitudes and hence can be represented by a "current sheet" model.  
 371 Jupiter's magnetosphere and the currents therein are inherently variable, which poses chal-  
 372 lenges for developing a suitable model. For simplicity, we initially adopt a widely-used  
 373 model of the "nominal" current sheet. This is the parameterized model of *Connerney*  
 374 [1981] which considers an axisymmetric disc of azimuthal currents in the magnetic equa-  
 375 tor. This model is defined by a half-width of  $2.5 R_J$ , inner radius of  $5 R_J$ , and current  
 376 sheet current density of  $225 \text{ nT}$  ( $\mu_0 I_0/2$ , where  $\mu_0$  is the permeability of free space and  $I_0$   
 377 is a reference current per unit length). An outer radius of  $50 R_J$  is also specified, but the  
 378 centrifugal equator at the  $5\text{--}10 R_J$  radial distance of the Io plasma torus is essentially the  
 379 same for any plausible value of the outer radius.

380 The bottom panel of Figure 7 compares the observed locations of the centrifugal  
 381 equator to the locations predicted by the combination of the truncated JRM09 internal  
 382 field model and the nominal current sheet model. The observed locations of the torus be-  
 383 yond  $5.5 R_J$  are now consistent with predictions. Furthermore, at the longitudes of each  
 384 of the four perijoves, the predicted locations of the two torus regions are separated by an  
 385 amount and direction comparable to the observed separations. However, the observed lo-  
 386 cations of the cold torus, which were predicted well prior to the inclusion of a current  
 387 sheet model, are now predicted acceptably, but not as well as before. Inclusion of the  
 388 nominal current sheet model has improved some aspects of the data-model comparison,  
 389 but worsened other aspects. On the whole, the agreement between observations and pre-  
 390 dictions for the combination of the truncated JRM09 internal field model and the nominal  
 391 current sheet model is promising.

392 We conclude that addition of a current sheet contribution to an internal magnetic  
 393 field model is necessary in order for a model to accurately predict the location of the cen-  
 394 trifugal equator for the "torus beyond  $5.5 R_J$ ". The current sheet is not needed to explain  
 395 the the cold torus location. This suggests that the current sheet model should not penetrate  
 396 into  $5 R_J$ . The combination of the truncated JRM09 internal field model and the nomi-  
 397 nal current sheet model of *Connerney* [1981] provides a promising, but imperfect, predic-  
 398 tion of the location of centrifugal equator. This is not unreasonable as the current sheet is  
 399 known to vary spatially and temporally in ways that are not represented by the idealized  
 400 current sheet model of *Connerney* [1981] [*Vogt et al.*, 2017].

## 401 5 Effects of variations in current sheet model parameters

402 The parameters of the nominal current sheet model are listed in the bottom of Ta-  
 403 ble 1. However, the real current sheet is likely more complex and variable than suggested  
 404 by this model, which would cause errors in the predictions of the nominal current sheet  
 405 model. To assess the degree to which changes in the values of the parameters of the nom-

406 final current sheet model change the predicted location of the centrifugal equator, we per-  
 407 form a series of simulations in which the values of these parameters are varied.

408 First, we vary the current sheet inner radius of  $5 R_J$  to 6, 7, and  $8 R_J$  while keep-  
 409 ing the half-width and current sheet density fixed at their nominal values. This steps  
 410 through the values of the inner radius from the inner density boundary of the IPT (around  
 411  $5 R_J$ ) through the outer density boundary (around  $8 R_J$ ). Results are shown in the top  
 412 row of Figure 8. Changes in the location of the centrifugal equator due to the simulated  
 413 variations in the current sheet inner radius are relatively small. In this idealized model,  
 414 the current sheet has limited effects on the location of the centrifugal equator within the  
 415 inner radius. Therefore, if the inner radius is moved out from  $5 R_J$  then the combination  
 416 of JRM09 and current sheet will better represent the data. *Pensionerov et al.* [2019] found  
 417 that a better match to the data was found using an inner radius of  $7 R_J$ . *Ridley and Holme*  
 418 [2016] found an inner radius of around  $4 R_J$  was a better fit. At small radial distances,  
 419 the centrifugal equator effectively remains at the location predicted by the internal field  
 420 model only.

421 Second, we vary the current sheet density ( $\mu_0 I_0/2$ ) of 225 nT to 125, 325, and 425  
 422 nT while keeping the inner radius and half-width fixed at their nominal values. The val-  
 423 ues are varied from 125 nT through 425 nT counting by 100 nT. This range was chosen  
 424 to contain the values for the current sheet found by *Vogt et al.* [2017] from fitting to the  
 425 Galileo data. Results are shown in the middle row of Figure 8. In this idealized model,  
 426 as the current sheet density increases, the displacement of the predicted location of the  
 427 centrifugal equator from the location predicted by the internal field-only model increases.  
 428 Changes are most apparent at radial distances greater than the inner radius of the current  
 429 sheet. For the values simulated here, these changes in location can be on the order of one  
 430 degree, which is substantial.

431 Third, we vary the current sheet half-width of  $2.5 R_J$  to 1.5, 3.5, and  $4.5 R_J$  while  
 432 keeping the inner radius and current sheet density fixed at their nominal values. These  
 433 values were chosen to be between 1 and  $5 R_J$  counting by  $1 R_J$  where the list of values  
 434 would include the initial value of  $2.5 R_J$ . Results are shown in the bottom row of Fig-  
 435 ure 8. In this idealized model, changes in the location of the centrifugal equator due to  
 436 simulated variations in the current sheet half-width are relatively small. A comparison of  
 437 all the test cases at  $6 R_J$  is shown in Figure 9. Although we test the parameters indepen-  
 438 dently, *Ridley and Holme* [2016] have shown that the values of  $D$  and  $\mu_0 I_0/2$  are covariant  
 439 and thus should be treated as a single parameter. This covariance does not change the re-  
 440 sults of this work, but it would be more physically realistic to vary  $D\mu_0 I_0/2$ , rather than  
 441 to vary both  $D$  and  $\mu_0 I_0/2$ .

442 In this idealized model of the current sheet, the predicted location of the centrifugal  
 443 equator is sensitive to the assumed value of the current sheet density, but is only weakly  
 444 sensitive to the assumed values of the current sheet inner radius and half-width. At this  
 445 stage, it is premature to consider the “best” set of parameters for this particular current  
 446 sheet model, which would be the set that gives the best agreement between observed and  
 447 predicted locations of the centrifugal equator. However, we note that none of the model  
 448 adjustments explored in Figure 8 yields what visual inspection would identify as an ap-  
 449 preciably better agreement between observations and predictions than the nominal model  
 450 shown in Figure 7.

## 451 6 Discussion

452 Ground-based imaging of the Io plasma torus has shown that the centrifugal equa-  
 453 tor of Jupiter’s magnetic field is warped from the idealized shape of a plane. Analysis of  
 454 four Juno radio occultation observations of the total electron content distribution in the Io  
 455 plasma torus has confirmed this finding. A dipolar magnetic field would produce a planar

456 centrifugal equator and cannot produce the observed structure. Furthermore, both ground-  
 457 based imaging and radio occultation observations show that the location of the centrifugal  
 458 equator at fixed longitude depends on radial distance. For example, the angular location of  
 459 the centrifugal equator has been observed to change by one degree between the cold torus  
 460 at  $5.3 R_J$  and the “torus beyond  $5.5 R_J$ ” (ribbon and warm torus) at  $5.9 R_J$ .

461 We modeled the location of the centrifugal equator using the VIP4 internal field  
 462 model of Jupiter’s internal magnetic field and compared these predictions to locations ob-  
 463 served in Juno radio occultation observations of the Io plasma torus. To determine the fit  
 464 of the model to the data we calculate the Root-Mean-Squared Error (RMSE). The RMSE  
 465 is calculated using the model output for a radial distance of  $5.3 R_J$  for the cold torus and  
 466  $5.9 R_J$  for the torus beyond  $5.5 R_J$ . This is repeated for each longitude. The RMSE for  
 467 predictions of the location of the centrifugal equator is  $0.54 \pm 0.20$  degrees for the cold  
 468 torus while it is  $1.35 \pm 0.50$  degrees for the torus beyond  $5.5 R_J$ .

469 Next, we modeled the location of the centrifugal equator using the JRM09 internal  
 470 field model of Jupiter’s internal magnetic field and compared these predictions to locations  
 471 observed in Juno radio occultation observations of the Io plasma torus. Terms beyond de-  
 472 gree 4 did not affect the predicted location of the centrifugal equator significantly. The  
 473 RMSE of the predictions of the location of the centrifugal equator is  $0.17 \pm 0.20$  degrees  
 474 for the cold torus and  $0.82 \pm 0.50$  degrees for the torus beyond  $5.5 R_J$ . Based on these  
 475 findings, we conclude that the JRM09 internal field model is an improvement over the ear-  
 476 lier VIP4 internal field model.

477 Reproduction of the observed large changes in the location of the centrifugal equa-  
 478 tor over short radial distances far from the planet with an internal magnetic field requires  
 479 considerable power in the high degree components of the magnetic field. This is incon-  
 480 sistent with plausible internal magnetic field models — not only their specific coefficient  
 481 values, but also their general spectral shape [Connerney *et al.*, 2018]. As previously sug-  
 482 gested by Herbert *et al.* [2008], magnetic fields induced by the flow of plasma in Jupiter’s  
 483 magnetosphere could cause variations in the location of the centrifugal equator over the  
 484 short length-scales required to reproduce the observations. We added the nominal cur-  
 485 rent sheet model of Connerney [1981] to the JRM09 internal field model, then modeled  
 486 the location of the centrifugal equator. The root-mean-squared error of predicted locations  
 487 of the centrifugal equator for the cold torus, which was  $0.17 \pm 0.20$  degrees prior to the  
 488 addition of the current sheet model, worsened to  $0.41 \pm 0.20$  degrees. The RMSE of pre-  
 489 dicted locations of the centrifugal equator for the torus beyond  $5.5 R_J$ , which was  $0.82 \pm$   
 490  $0.50$  degrees prior to the addition of the current sheet model, improved to  $0.49 \pm 0.50$  de-  
 491 grees. As can be seen in the bottom panel of Figure 7, the inclusion of the current sheet  
 492 model increases the magnitude of the rate of change of angular offset with radial distance.  
 493 This characteristic explains why inclusion of the current sheet model is able to improve  
 494 data-model agreement for the torus beyond  $5.5 R_J$ , but worsen it for the cold torus.

495 On the whole, the combination of the truncated JRM09 internal field model and the  
 496 nominal current sheet model of Connerney [1981] provides promising, but imperfect, pre-  
 497 dictions of the location of centrifugal equator for the radial distances of the Io plasma  
 498 torus. By implication, this combination of internal and induced field models provides  
 499 an accurate description of the magnetic field environment in the equatorial regions of  
 500 Jupiter’s inner magnetosphere. The improvements obtained in predictions of the location  
 501 of the centrifugal equator by advancing from the VIP4 internal field model to the JRM09  
 502 internal field model, and from adding the nominal current sheet model to the JRM09 in-  
 503 ternal field model, are strikingly illustrated in the top panel of Figure 10.

504 Overall, it appears that magnetic field conditions around  $5.3 R_J$  (representative ra-  
 505 dial distance of the cold torus) are adequately represented by an internal field model with-  
 506 out the need for appreciable contributions from the external field generated by the magne-  
 507 toospheric current sheet. Yet magnetic field conditions around  $5.9 R_J$  (representative radial

508 distance of the torus beyond  $5.5 R_J$ ) require contributions from both an internal field and  
 509 an external field. This pair of results places constraints on the properties of the magneto-  
 510 spheric current sheet during the Juno epoch.

511 The nominal current sheet model has three significant parameters: half-width, in-  
 512 ner radius, and current sheet density. The predicted location of the centrifugal equator is  
 513 most sensitive to the adopted value of the current sheet density, but is relatively insensitive  
 514 to the adopted values of half-width and inner radius. However, the effects of the current  
 515 sheet on the location of the centrifugal equator are weak at distances closer to Jupiter than  
 516 the inner radius of the current sheet. Limited exploration of the consequences of varying  
 517 the parameters of this current sheet model did not yield predicted locations of the cen-  
 518 trifugal equator that appeared appreciably better than the predictions generated using the  
 519 nominal set of parameters.

520 Impressive similarities exist between the structure of the centrifugal equator ob-  
 521 served by ground-based imaging and by Juno radio occultation observations of the Io  
 522 plasma torus, as shown in the bottom panel of Figure 10. For the ground-based imaging  
 523 results of Schneider and Trauger [1995], this panel shows the observed offset of the ribbon  
 524 from the location of the centrifugal equator predicted by their offset tilted dipole (OTD)  
 525 model of the internal magnetic field. For Juno radio occultation observations, this panel  
 526 shows the observed offsets of the cold torus and the torus beyond  $5.5 R_J$  from the loca-  
 527 tion of the centrifugal equator predicted by the dipolar approximation to the VIP4 internal  
 528 field model of the internal magnetic field. The correspondence between the ribbon offsets  
 529 found by ground-based imaging and the cold torus offsets found by Juno radio occultation  
 530 observations is remarkable. It is also somewhat challenging to interpret as the ribbon is a  
 531 distinctive feature in ground-based imaging, but not in Juno radio occultation observations,  
 532 whereas the cold torus is a distinctive feature in Juno radio occultation observations, but  
 533 not in ground-based imaging. We defer further interpretation of this intriguing result to  
 534 future work.

## 535 7 Conclusions

536 Several predictions concerning the magnetosphere of Jupiter arise from the results of  
 537 this work.

- 538 1. Future Juno radio occultation observations of the Io plasma torus should yield loca-  
 539 tions of the cold torus and the torus beyond  $5.5 R_J$  that agree with the locations of  
 540 the centrifugal equator that are predicted by the combination of the JRM09 internal  
 541 field model and the nominal current sheet model.
- 542 2. Future Juno radio occultation observations of the Io plasma torus at longitudes al-  
 543 ready sampled by previous Juno radio occultation observations should yield the  
 544 same locations of the cold torus and the torus beyond  $5.5 R_J$  as in those previous  
 545 observations.
- 546 3. By adjusting values of model parameters to optimize agreement between predic-  
 547 tions and observations for the location of the centrifugal equator, it should be possi-  
 548 ble to place constraints on the properties of the current sheet in Jupiter's magneto-  
 549 sphere, particularly the current density.
- 550 4. The combination of the JRM09 internal field model and a current sheet model  
 551 should provide an accurate description of the Io plasma torus in the equatorial re-  
 552 gions of Jupiter's inner magnetosphere.
- 553 5. The effect of the current sheet on the centrifugal equator should increase substan-  
 554 tially from 5 to  $6 R_J$ . For instance, the ribbon feature of the Io plasma torus, which  
 555 is thought to be associated with the change in the radial temperature gradient, may  
 556 be the boundary between inner regions that are primarily affected by the inter-

557       nal field and outer regions that are significantly affected by flows of hot magneto-  
 558       spheric plasma.

559       Several potentially fruitful avenues for further research arise from the results of this  
 560       work.

- 561       1. Synthesis of findings on the location of the Io plasma torus from ground-based  
       562       imaging and Juno radio occultation observations. This would improve understand-  
       563       ing of the Io plasma torus' structure and role in Jupiter's magnetosphere. However,  
       564       differences in the detectability of the distinct torus regions between these two mea-  
       565       surement techniques presents both challenges and opportunities.
- 566       2. Investigation of the predicted location of the centrifugal equator for different cur-  
       567       rent sheet models and different sets of model parameters. The Juno radio occulta-  
       568       tion observations present an opportunity to indirectly test proposed current sheet  
       569       models, to reject unsuccessful models, and to place constraints on plausible param-  
       570       eter values for successful models. This would support a range of investigations into  
       571       plasma dynamics in the inner magnetosphere and associated topics.
- 572       3. Assessment of the effect of temperature anisotropy on torus location. If the plasma  
       573       temperature is highly anisotropic ( $T_{\perp} \gg T_{\parallel}$ ) then plasma in the torus will be cen-  
       574       tered around the magnetic equator, not the centrifugal equator [Vasyliunas, 1983;  
       575       Khurana *et al.*, 2004]. Current sheet effects and temperature anisotropy effects can  
       576       both alter the torus location from that predicted by an internal field model.
- 577       4. Acquisition and analysis of additional Juno radio occultation observations of the Io  
       578       plasma torus. Additional observations will fill in gaps in the observed longitudinal  
       579       structure, as well as provide repeat coverage at some longitudes. This would bet-  
       580       ter characterize the spatial structure of the Io plasma torus, as well as its temporal  
       581       variability.

### 582       **Acknowledgments**

583       The authors would like to thank two anonymous reviewers for their reviews of this manuscript.  
 584       No new data products were introduced in this article. The Juno data products used in  
 585       this article were previously published in Phipps *et al.* [2018] and Phipps *et al.* [2019].  
 586       The data used in this work are publicly available on the NASA Planetary Data System at  
 587       [http://pds-atmospheres.nmsu.edu/data\\_and\\_services/atmospheres\\_data/JUNO/gravity.html](http://pds-atmospheres.nmsu.edu/data_and_services/atmospheres_data/JUNO/gravity.html).  
 588       The authors would also like to thank Fran Bagenal for useful discussions related to this  
 589       manuscript. The work of D. Buccino, M. Parisi and O. Yang was carried out at the Jet  
 590       Propulsion Laboratory, California Institute of Technology, under a contract with the Na-  
 591       tional Aeronautics and Space Administration. Government sponsorship acknowledged.  
 592       This work was supported in part by NASA award 80NSSC19K0818.

### 593       **References**

- 594       Acuna, M. H., and N. F. Ness (1976), The main magnetic field of Jupiter, *J. Geophys.*  
 595       *Res.*, 81(16), 2917, doi:10.1029/JA081i016p02917.
- 596       Bagenal, F. (1994), Empirical model of the Io plasma torus: Voyager measurements, *J.*  
 597       *Geophys. Res.*, 99, 11,043–11,062, doi:10.1029/93JA02908.
- 598       Bagenal, F. (2013), *Planetary Magnetospheres*, pp. 251–307, Springer Netherlands, Dor-  
 599       recht.
- 600       Bagenal, F., and J. D. Sullivan (1981), Direct plasma measurements in the Io  
 601       torus and inner magnetosphere of Jupiter, *J. Geophys. Res.*, 86, 8447–8466, doi:  
 602       10.1029/JA086iA10p08447.
- 603       Chapman, S., and J. Bartels (1940), *Geomagnetism*, London: Oxford Univ. Press.
- 604       Connerney, J. E. P. (1981), The magnetic field of Jupiter - A generalized inverse approach,

- 605                   *J. Geophys. Res.*, 86, 7679–7693, doi:10.1029/JA086iA09p07679.
- 606                   Connerney, J. E. P. (1993), Magnetic fields of the outer planets, *J. Geophys. Res.*, 98, 18,  
607                   doi:10.1029/93JE00980.
- 608                   Connerney, J. E. P., M. H. Acuna, and N. F. Ness (1981), Modeling the Jovian  
609                   current sheet and inner magnetosphere, *J. Geophys. Res.*, 86, 8370–8384, doi:  
610                   10.1029/JA086iA10p08370.
- 611                   Connerney, J. E. P., M. H. Acuña, N. F. Ness, and T. Satoh (1998), New models of  
612                   Jupiter's magnetic field constrained by the Io flux tube footprint, *J. Geophys. Res.*, 103,  
613                   11,929–11,940, doi:10.1029/97JA03726.
- 614                   Connerney, J. E. P., S. Kotsiaros, R. J. Oliversen, J. R. Espley, J. L. Joergensen, P. S. Joer-  
615                   gensen, J. M. G. Merayo, M. Herceg, J. Bloxham, K. M. Moore, S. J. Bolton, and S. M.  
616                   Levin (2018), A New Model of Jupiter's Magnetic Field From Juno's First Nine Orbits,  
617                   *Geophys. Res. Lett.*, 45, 2590–2596, doi:10.1002/2018GL077312.
- 618                   Goertz, C. K. (1976), The current sheet in Jupiter's magnetosphere, *J. Geophys. Res.*,  
619                   81(19), 3368, doi:10.1029/JA081i019p03368.
- 620                   Grodent, D., B. Bonfond, J.-C. GéRard, A. Radioti, J. Gustin, J. T. Clarke, J. Nichols,  
621                   and J. E. P. Connerney (2008), Auroral evidence of a localized magnetic anomaly in  
622                   Jupiter's northern hemisphere, *J. Geophys. Res. (Space Physics)*, 113, A09201, doi:  
623                   10.1029/2008JA013185.
- 624                   Herbert, F., N. M. Schneider, and A. J. Dessler (2008), New description of  
625                   Io's cold plasma torus, *J. Geophys. Res. (Space Physics)*, 113, A01208, doi:  
626                   10.1029/2007JA012555.
- 627                   Hess, S. L. G., B. Bonfond, P. Zarka, and D. Grodent (2011), Model of the Jovian mag-  
628                   netic field topology constrained by the Io auroral emissions, *J. Geophys. Res. (Space*  
629                   *Physics)*, 116(A5), doi:10.1029/2010JA016262.
- 630                   Hill, T. W., A. J. Dessler, and F. C. Michel (1974), Configuration of the Jovian magneto-  
631                   sphere, *Geophys. Res. Lett.*, 1, 3–6, doi:10.1029/GL001i001p00003.
- 632                   Khurana, K. K. (1992), A Generalized Hinged-Magnetodisc Model of Jupiter's Nightside  
633                   Current Sheet, *J. Geophys. Res.*, 97(A5), 6269–6276, doi:10.1029/92JA00169.
- 634                   Khurana, K. K. (1997), Euler potential models of Jupiter's magnetospheric field, *J. Geo-  
635                   phys. Res.*, 102(A6), 11,295–11,306, doi:10.1029/97JA00563.
- 636                   Khurana, K. K., M. G. Kivelson, V. M. Vasiliunas, N. Krupp, J. Woch, A. Lagg, B. H.  
637                   Mauk, and W. S. Kurth (2004), *The configuration of Jupiter's magnetosphere*, pp. 593–  
638                   616, Cambridge, UK: Cambridge University Press.
- 639                   Kivelson, M. G., and F. Bagenal (2014), Chapter 7 - planetary magnetospheres, in  
640                   *Encyclopedia of the Solar System (Third Edition)*, edited by T. Spohn, D. Breuer,  
641                   and T. V. Johnson, third edition ed., pp. 137 – 157, Elsevier, Boston, doi:  
642                   https://doi.org/10.1016/B978-0-12-415845-0.00007-4.
- 643                   Pensionerov, I. A., I. I. Alexeev, E. S. Belenkaya, J. E. P. Connerney, and S. W. H.  
644                   Cowley (2019), Model of Jupiter's Current Sheet With a Piecewise Current Den-  
645                   sity, *Journal of Geophysical Research (Space Physics)*, 124(3), 1843–1854, doi:  
646                   10.1029/2018JA026321.
- 647                   Phipps, P. H. (2019), Distribution of plasma in the Io plasma torus from radio occultations  
648                   during the Juno epoch, Ph.D. thesis, Boston University, Massachusetts, USA.
- 649                   Phipps, P. H., and P. Withers (2017), Radio occultations of the Io plasma torus  
650                   by Juno are feasible, *J. Geophys. Res. (Space Physics)*, 122, 1731–1750, doi:  
651                   10.1002/2016JA023447.
- 652                   Phipps, P. H., P. Withers, B. D. R., and Y.-M. Yang (2018), Distribution of plasma in the  
653                   Io plasma torus as seen by radio occultation during Juno Perijove 1, *J. Geophys. Res.*  
654                   *(Space Physics)*, 123, 6207–6222, doi:10.1029/2017JA025113.
- 655                   Phipps, P. H., P. Withers, D. R. Buccino, Y.-M. Yang, and M. Parisi (2019), Variations in  
656                   the Density Distribution of the Io Plasma Torus as Seen by Radio Occultations on Juno  
657                   Perijoves 3, 6, and 8, *Journal of Geophysical Research: Space Physics*, 124(7), 5200–  
658                   5221, doi:10.1029/2018JA026297.

- 659 Ridley, V. A., and R. Holme (2016), Modeling the Jovian magnetic field and its secular  
660 variation using all available magnetic field observations, *Journal of Geophysical Re-*  
661 *search (Planets)*, 121(3), 309–337, doi:10.1002/2015JE004951.
- 662 Schneider, N. M., and J. T. Trauger (1995), The Structure of the Io Torus, *Astrophys. J.*,  
663 450, 450, doi:10.1086/176155.
- 664 Thomas, N., F. Bagenal, T. W. Hill, and J. K. Wilson (2004), The Io neutral clouds and  
665 plasma torus, in *Jupiter: The Planet, Satellites and Magnetosphere*, edited by F. Bage-  
666 nal, T. E. Dowling, and W. B. McKinnon, pp. 561–591, Cambridge, UK: Cambridge  
667 University Press.
- 668 Vasyliunas, V. M. (1983), *Plasma distribution and flow*, pp. 395–453, Cambridge, UK:  
669 Cambridge University Press.
- 670 Vogt, M. F., E. J. Bunce, J. D. Nichols, J. T. Clarke, and W. S. Kurth (2017), Long-Term  
671 Variability of Jupiter's Magnetodisk and Implications for the Aurora, *J. Geophys. Res.*  
(Space Physics), 122, 12,090–12,110, doi:10.1002/2017JA024066.
- 672

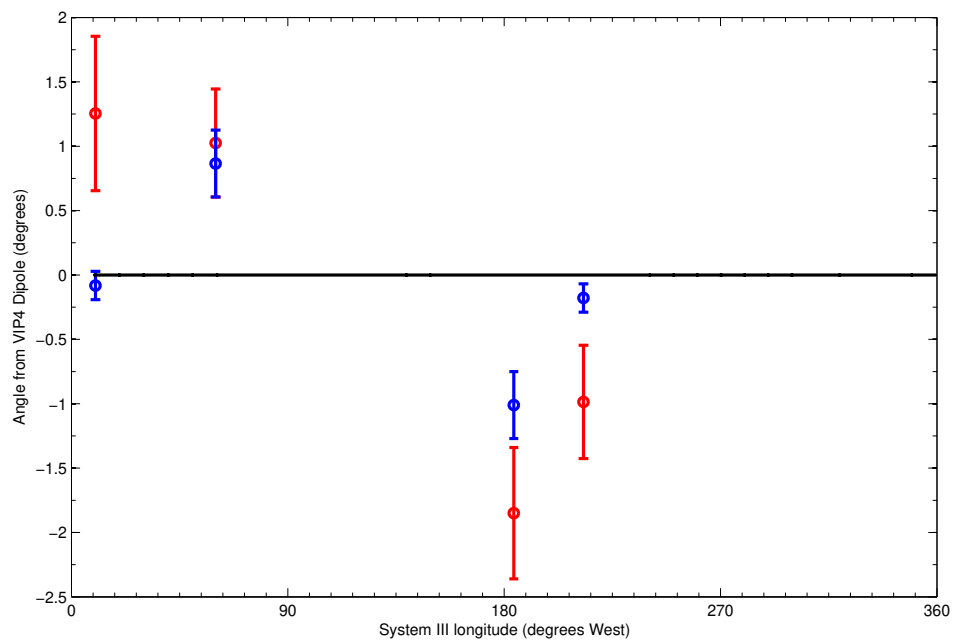
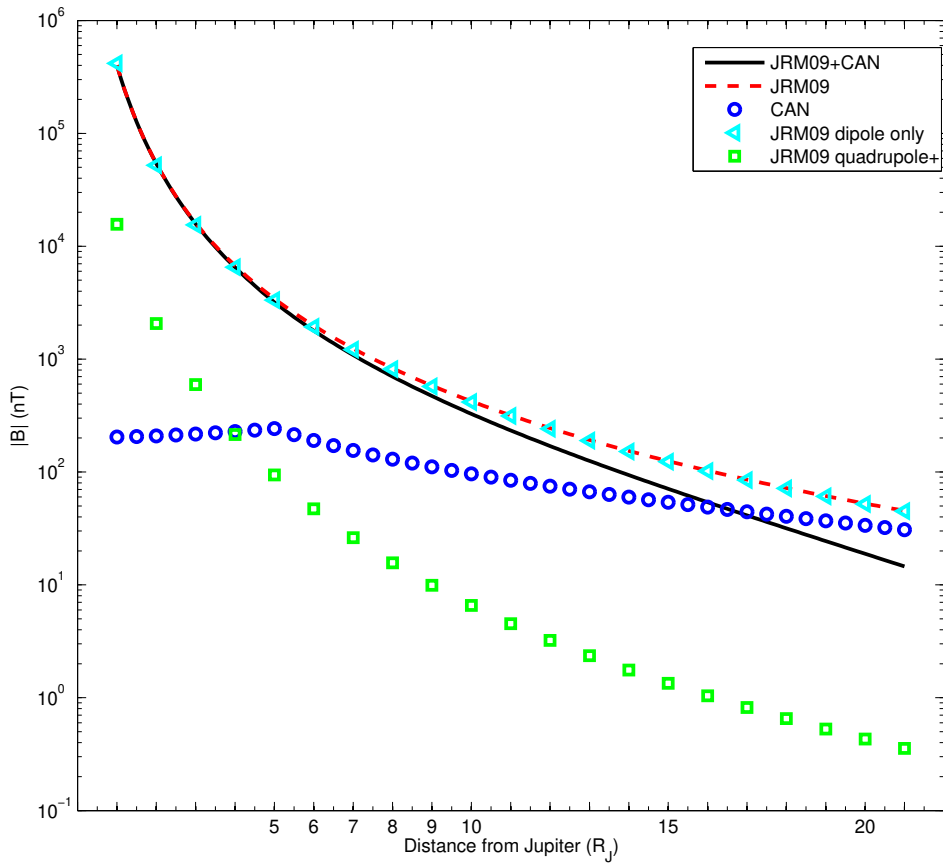
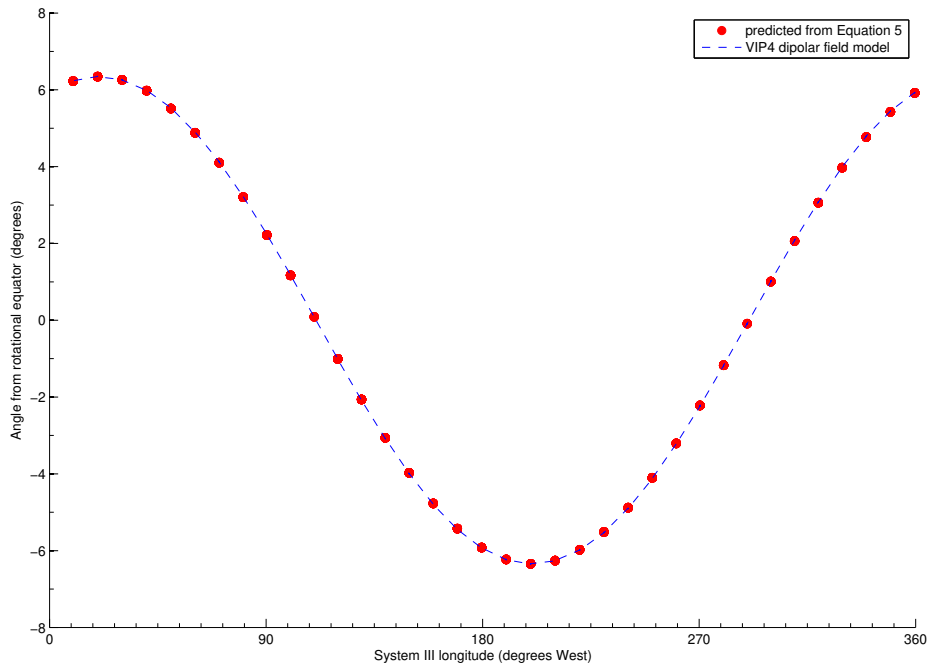


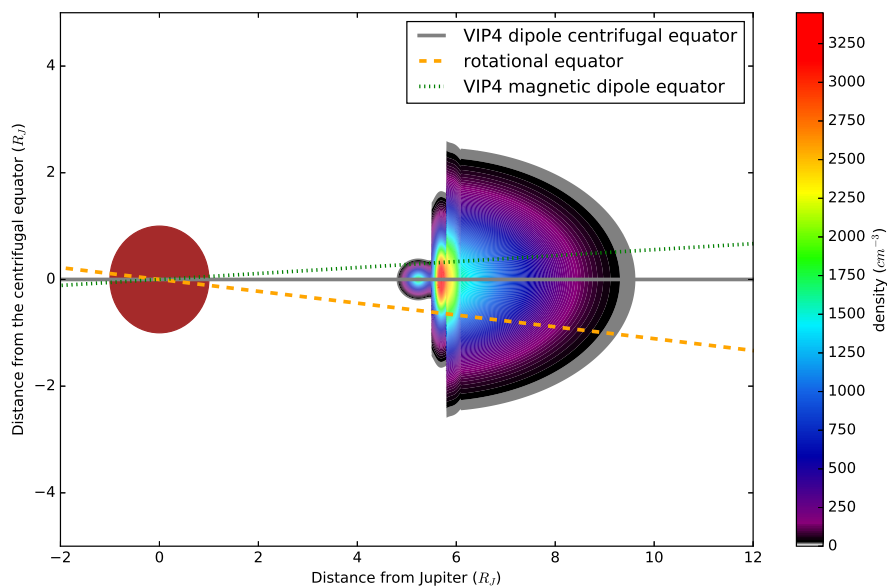
**Figure 1.** Observations of the centrifugal equator from Juno radio occultations of the Io plasma torus. Blue symbols and red symbols are Juno radio occultation observations of the cold torus and the torus beyond 5.5  $R_J$ , respectively.



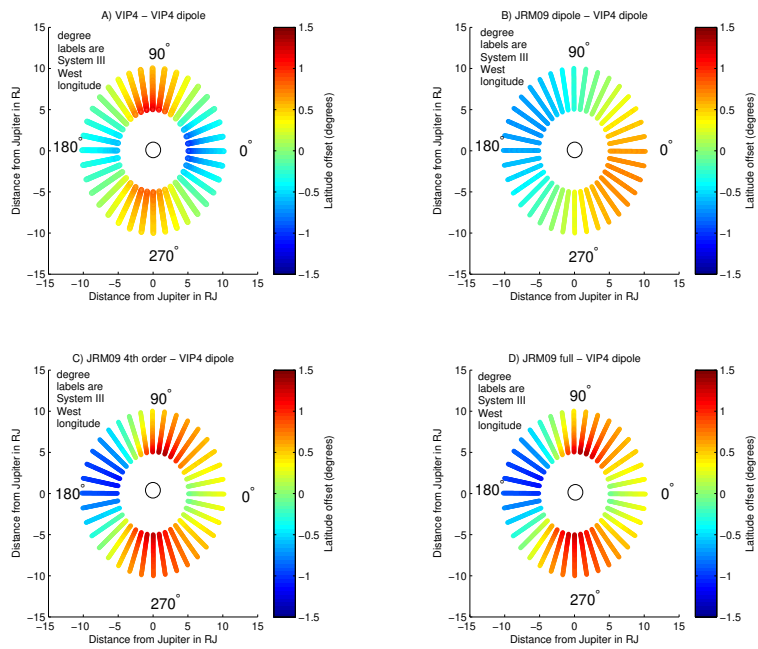
676 **Figure 2.** Model predictions for the magnitude of the magnetic field in the magnetic equator. Results are  
 677 shown for the JRM09+CAN (black solid line), JRM09 (red dashed line), JRM09 dipole (cyan triangles),  
 678 JRM09 quadrupole and above (green squares), and CAN-only (blue circles) models.



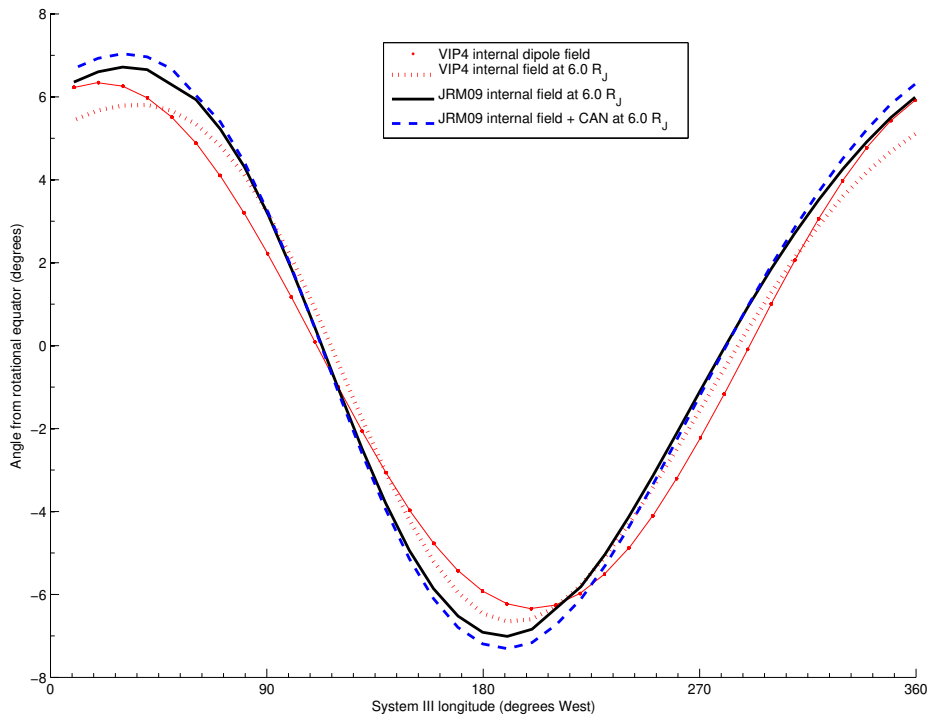
679 **Figure 3.** The predicted location of the centrifugal equator relative to the rotational equator.  
680 Red circles show the prediction from the dipolar approximation to the VIP4 internal field model by Equation 5.  
681 The blue dashed line shows the prediction from field line tracing using the dipolar approximation to the VIP4 model.



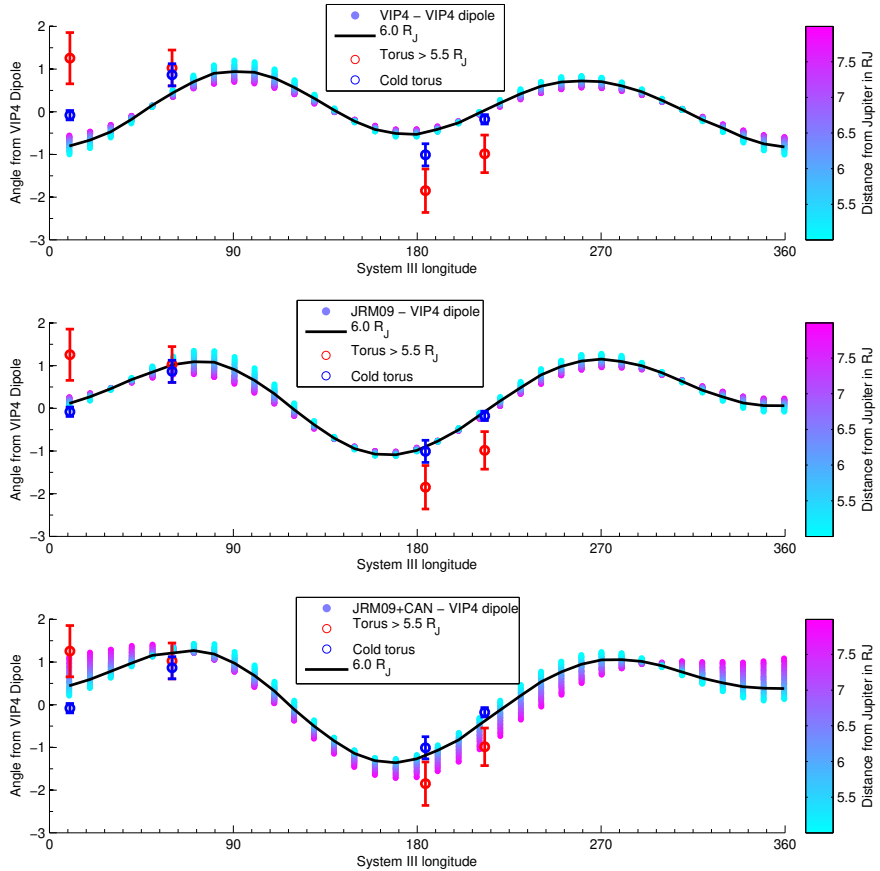
682      **Figure 4.** Schematic of the location of the centrifugal equator with respect to the rotational and magnetic  
683      equators in the dipole approximation. Colored regions show plasma density according to the model B from  
684      *Phipps et al. [2018]*.



685 **Figure 5.** Model predictions for the centrifugal equator relative to the centrifugal equator of the dipolar  
 686 approximation to the VIP4 internal field model. Results are shown between 5 and 10  $R_J$  at intervals of 10  
 687 degrees in longitude as viewed from above Jupiter's south pole looking north. A. The full VIP4 internal field  
 688 model. B. The dipolar approximation to the JRM09 internal field model. C. The degree 4 truncation of the  
 689 JRM09 internal field model. D. The full JRM09 internal field model.



690 **Figure 6.** The location of the centrifugal equator at  $6 R_J$  relative to the rotational equator, as predicted for  
 691 the dipolar approximation to the VIP4 internal field model (red dots joined by solid red line), the full VIP4  
 692 internal field model (red dashed line), the JRM09 4th order internal field model (black solid line), and the  
 693 JRM09 internal field plus current sheet model (blue dashed line).



694 **Figure 7.** Comparison of observed and predicted locations of the centrifugal equator relative to the cen-  
 695 trifugal equator of the dipolar approximation to the VIP4 internal field model. Blue symbols and red symbols  
 696 are Juno radio occultation observations of the cold torus and the torus beyond  $5.5 R_J$ , respectively. Colored  
 697 swaths are predictions made between 5 and 8  $R_J$  at intervals of 10 degrees in longitude. The black line high-  
 698 lights the prediction for a radial distance of 6  $R_J$ . (top) Predictions from the full VIP4 internal field model.  
 699 (middle) Predictions from the degree 4 truncation of the JRM09 internal field model. (bottom) Predictions  
 700 from the combination of the degree 4 truncation of the JRM09 internal field model and the nominal current  
 701 sheet model.

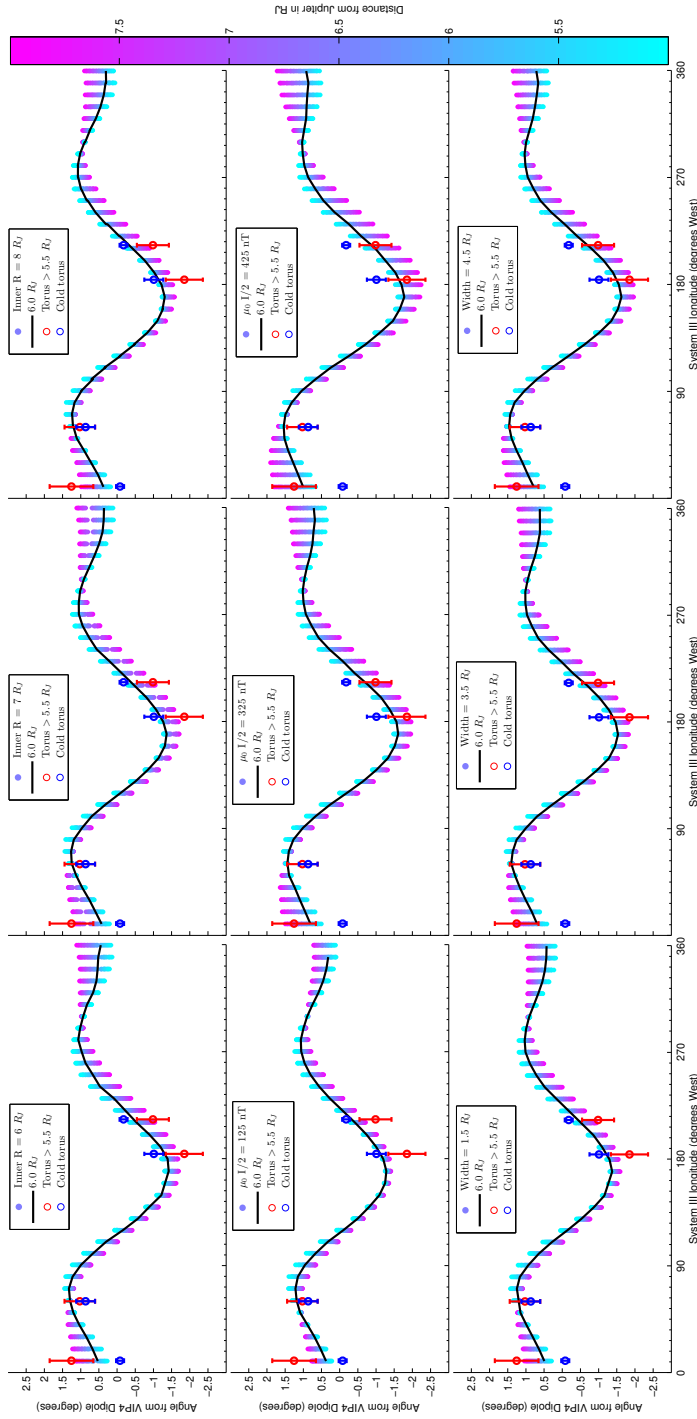
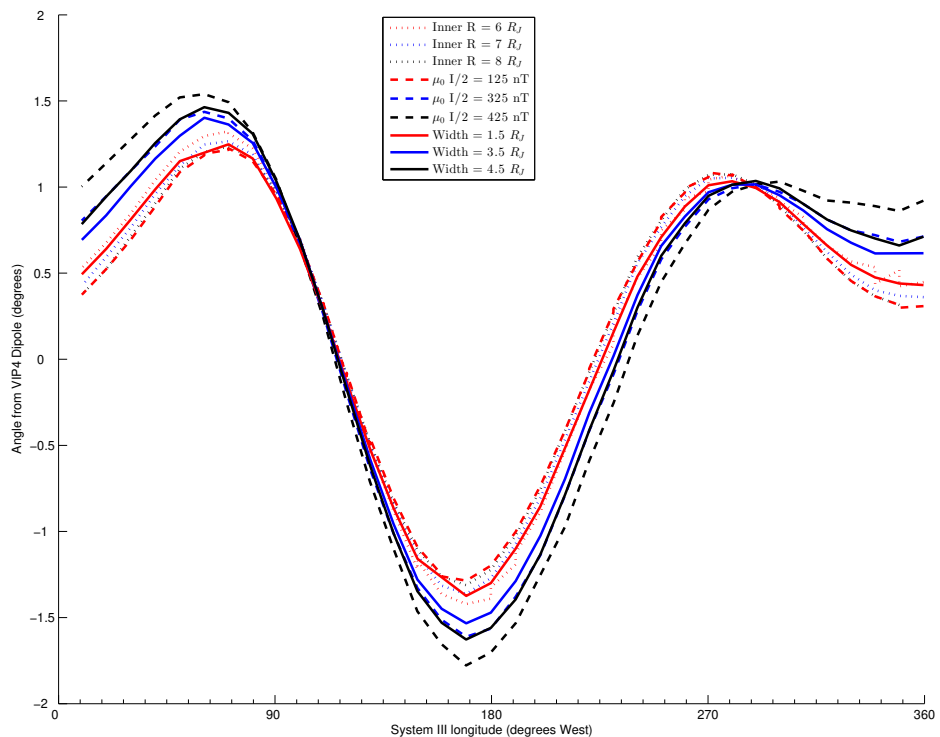
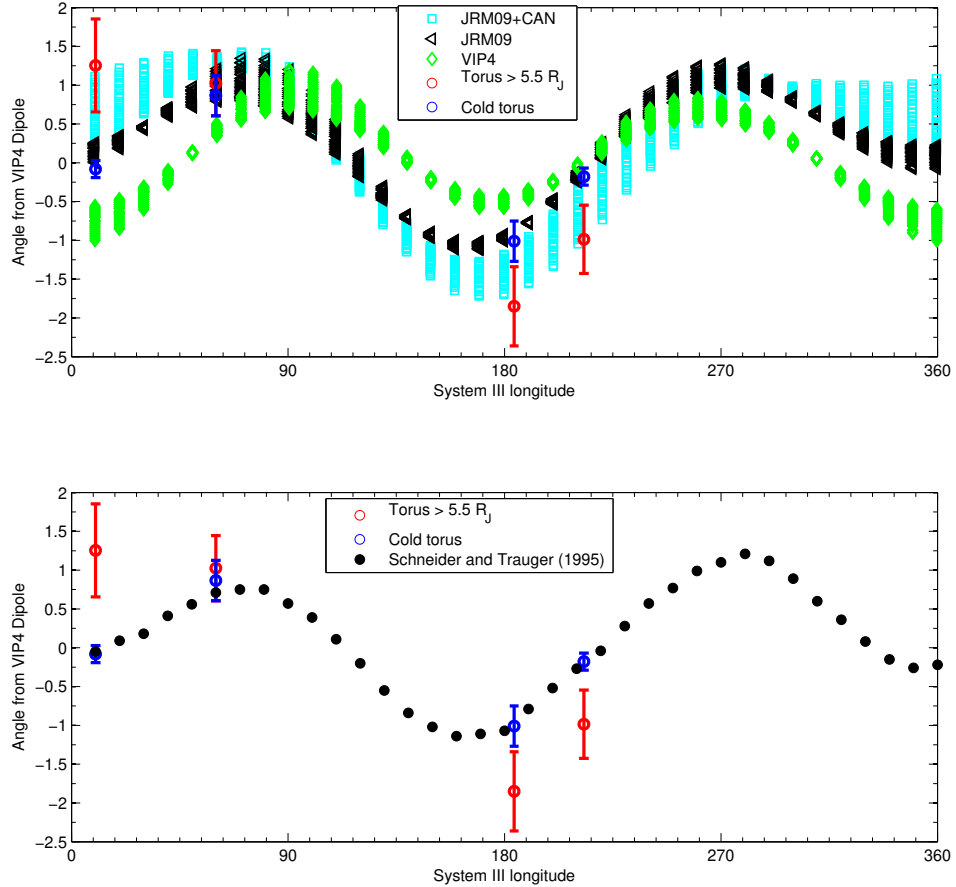


**Figure 8.** As the bottom panel of Figure 7 using JRM09 internal field model, but for different current sheet models. Note that the radial distances shown has expanded from 5–8  $R_J$  in Figure 7 to 5–10  $R_J$  here. In the top row, the current sheet model uses inner radial distances of 6, 7, and 8  $R_J$  instead of the nominal 5  $R_J$ . All other parameters have their nominal values. In the middle row, the current sheet model uses initial magnetic field values ( $\mu_0 I_0/2$ ) of 125, 325, and 425 nT instead of the nominal 225 nT. All other parameters have their nominal values. In the bottom row, the current sheet model uses half-widths of 1.5, 3.5, and 4.5  $R_J$  instead of the nominal 2.5  $R_J$ . All other parameters have their nominal values.



702 **Figure 9.** Dependence on longitude of values at  $6 R_J$  for all nine CAN tests shown in Figure 8. The dotted  
 703 lines show variation in the CAN inner radius, the dashed lines show variations in the CAN current density,  
 704 and the solid lines show variation in the CAN half-width.



705 **Figure 10.** (top) Observed and predicted locations of the centrifugal equator. Blue symbols and red symbols  
 706 are Juno radio occultation observations of the cold torus and the torus beyond  $5.5 R_J$ , respectively.  
 707 Predicted values are from the full VIP4 internal field model (green), the truncated JRM09 internal field  
 708 model (black), and the combination of the truncated JRM09 internal field model and the nominal current  
 709 sheet model (cyan) as shown in Figure 7. Predictions are shown for radial distances of 5–8  $R_J$ . (bottom)  
 710 Comparison of the location of the centrifugal equator as determined by ground-based imaging and Juno radio  
 711 occultation observations. Blue symbols and red symbols are Juno radio occultation observations of the cold  
 712 torus and the torus beyond  $5.5 R_J$ , respectively. These show location relative to the centrifugal equator of the  
 713 dipolar approximation to the VIP4 internal field model. Black symbols are ground-based imaging observa-  
 714 tions of the ribbon by Schneider and Trauger [1995]. These show location relative to the offset tilted dipole  
 715 (OTD) model used by Schneider and Trauger [1995].

<sup>716</sup> **Table 1.** The top portion of this table lists parameters of the dipolar approximations to the VIP4 and JRM09  
<sup>717</sup> models. The bottom portion of this table lists the parameters of the CAN model.

Internal Model	M Gauss	$\theta_M$ degrees	$\lambda_{III}$ degrees
VIP4	4.264	9.6	200.8
JRM09	4.170	10.31	196.61
External Model	$\mu_0 I_0 / 2$ nT	D $R_J$	Inner Radius $R_J$
<i>Connerney et al. [1981]</i>	225	2.5	5

718      **Table 2.** Offsets ( $\alpha$ ) of observed locations of torus regions from the centrifugal equator predicted by the  
 719      dipolar approximation to the VIP4 model. Uncertainties are also listed ( $\sigma$ ). Values are from *Phipps et al.*  
 720      [2018] (PJ1) and *Phipps et al.* [2019] (PJ3, PJ6, and PJ8).

Perijove	cold torus		torus $> 5.5 R_J$	
	$\alpha$ degrees	$\sigma$ degrees	$\alpha$ degrees	$\sigma$ degrees
Perijove 1	-0.90	0.10	-1.70	0.20
Perijove 3	0.79	0.26	1.47	0.41
Perijove 6	-0.19	0.11	-0.91	0.44
Perijove 8	0.05	0.12	1.08	0.60